Enhanced four-wave mixing in graphene-silicon slow-light photonic crystal waveguides

Hao Zhou, Tingyi Gu, James F. McMillan, Nicholas Petrone, Arend van der Zande, James C. Hone, Mingbin Yu, Guoqiang Lo, Dim-Lee Kwong, Guoying Feng, Shouhuan Zhou, and Chee Wei Wong

Citation: Applied Physics Letters **105**, 091111 (2014); doi: 10.1063/1.4894830
View online: http://dx.doi.org/10.1063/1.4894830
View Table of Contents: http://scitation.aip.org/content/aip/journal/apl/105/9?ver=pdfcov
Published by the AIP Publishing

Enhanced four-wave mixing in graphene-silicon slow-light photonic crystal waveguides

Hao Zhou,[1,2,a)] Tingyi Gu,[2,a)] James F. McMillan,[2] Nicholas Petrone,[3] Arend van der Zande,[3] James C. Hone,[3] Mingbin Yu,[4] Guoqiang Lo,[4] Dim-Lee Kwong,[4] Guoying Feng,[1] Shouhuan Zhou,[1,5] and Chee Wei Wong[2,a)]
[1]*College of Electronic Information, Sichuan University, Chengdu 610064, China*
[2]*Optical Nanostructures Laboratory, Columbia University, New York, New York 10027, USA*
[3]*Mechanical Engineering, Columbia University, New York, New York 10027, USA*
[4]*The Institute of Microelectronics, Singapore 117685, Singapore*
[5]*North China Research Institute of Electro-Optics, Beijing 100015, China*

(Received 18 June 2014; accepted 25 August 2014; published online 5 September 2014)

We demonstrate the enhanced four-wave mixing of monolayer graphene on slow-light silicon photonic crystal waveguides. 200-μm interaction length, a four-wave mixing conversion efficiency of -23 dB is achieved in the graphene-silicon slow-light hybrid, with an enhanced 3-dB conversion bandwidth of about 17 nm. Our measurements match well with nonlinear coupled-mode theory simulations based on the measured waveguide dispersion, and provide an effective way for all-optical signal processing in chip-scale integrated optics. © *2014 AIP Publishing LLC*.
[http://dx.doi.org/10.1063/1.4894830]

Recently, graphene, with its unique dispersionless and broadband band structure, provides an alternative platform for condensed matter physics and nanoscale devices including electronic, thermal, mechanical, and photonic applications. In the optical domain, exciting graphene enhanced applications include ultrafast mode-locking, modulators, detectors, photovoltaics, and optical frequency conversion.[1–6] Frequency conversion based on four-wave mixing (FWM) in mesoscopic devices has been examined in silicon nanowires and photonic crystal waveguides (PhCWGs).[7–10] In the communications (C) band, the bulk Kerr coefficient n_2 of silicon ($\sim 4 \times 10^{-18}$ m^2/W) can achieve enhanced four-wave mixing with engineered phase-matching, long waveguides, and/or slow group velocity interactions in engineered PhCWGs.[11–15] Graphene has even larger third-order nonlinearity susceptibility, a few orders of magnitude larger than bulk silicon and other semiconductors, with a corresponding Kerr coefficient $\sim 10^{-13}$ m^2/W. FWM is observed in graphene recently,[4,16–18] such as with microcavities and detuning within the cavity linewidth.[4] With the wider bandwidth waveguide implementation, here, we show the experimental observations of FWM in graphene-photonic crystal waveguides. Our measurements demonstrated up to a 17 nm (3-dB) conversion bandwidth in the slow-light region and 2D efficiency maps of the graphene-silicon idler conversion with a maximum -23 dB conversion efficiency, matching well with our theoretical modeling.

Inset of Fig. 1(a) shows the scanning electron micrograph (SEM) of the air-bridged silicon photonic crystal nanomembrane of 250 nm thickness and with monolayer graphene transferred on the top surface. The PhCWG consists of a missing row of holes in a W1 configuration with dispersion examined earlier,[19] fabricated by deep-ultraviolet optical lithography and with an effective cross-sectional model area (A_{eff}) about 0.55 μm^2. In our measurements here, the PhCWG total length is 200 μm. The monolayer graphene is grown by chemical vapor deposition (CVD) and wet-transferred onto the W1 PhCWG.[20,21] The central PhCWG area is covered by large-area monolayer graphene for evanescent-field graphene interaction. Raman spectroscopy is used to identify the single-layer graphene, with five selected Raman spectra shown in Fig. 1(a). Excited by a 532 nm wavelength laser, most of the graphene area has a *G* peak full-width half-maximum (FWHM) about 20 cm^{-1}, a *2D* peak FWHM about 38 cm^{-1}, and a *2D-to-G* peak intensity ratio ($\sim$2). This indicates the PhCWG is covered by uniform monolayer graphene.[22,23] The transmission of the chip is tested by a tunable laser (Ando AQ4321A) scanning from 1510 nm to 1555 nm, as shown in Fig. 1(b). The transmission before (red solid line) and after (blue solid line) transferred with graphene are presented. The group index of graphene-PhCWG is measured by the phase-delay method (green dots) and fitted by black line.[12] This transferred graphene layer has an intrinsic absorption of $\sim$0.05 dB/μm (or about 10 dB) for this sample, at 1510 nm and far from the slow-light band edge.

Fig. 2(a) shows the experimental setup used to achieve the degenerate FWM in the graphene-PhCWG. Two continuous-wave tunable lasers are amplified by two erbium-doped fiber amplifiers (EDFA; IPG EDA-3K-C, and Amonis AEDFA-PA-35-B-FA), serving as the pump and signal sources, respectively. A 50:50 optical fiber coupler combines the pump and signal prior to coupling into the graphene-PhCWG sample with a lensed fiber coupler. The coupling loss is about 4 dB, for a maximum pump power coupled into the waveguide of about 17 dBm. Another lensed fiber is placed after the waveguide to collect the output into an optical spectrum analyzer (OSA; Advantest Q8384). This all-fiber system is very robust. Before we mount the chips, the fiber to fiber transmission measurement is taken to observe the loop transmission as the background transmission in order to

[a)]Electronic addresses: hz2299@columbia.edu; tg2342@columbia.edu; and cww2104@columbia.edu

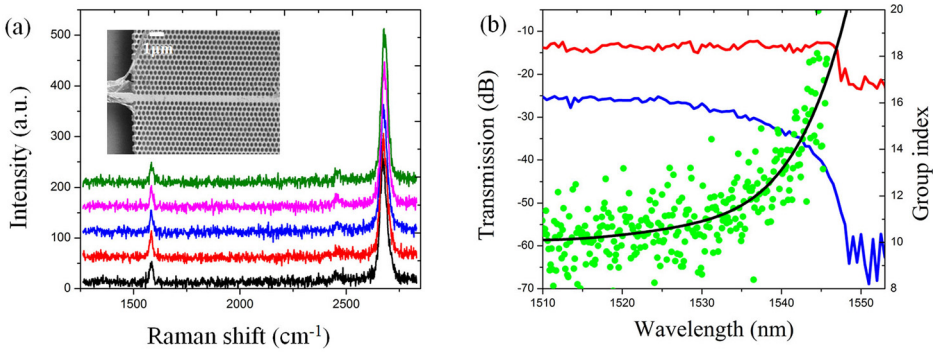

FIG. 1. The Raman spectra, transmission spectra, and group index of the Graphene-PhCWG device. (a) Five selected Raman spectra of the graphene on PhCWG; (b) Transmission spectra before (red solid line) and after (blue solid line) graphene transfer as well as the measured group index of graphene-PhCWG. Green dots are the measured group index of the graphene-PhCWG and the black line shows the fitted group index. Inset in (a) is the SEM of the graphene-PhCWG device. The central area is continuously covered by large-area monolayer graphene.

obtain the actual chip transmission. The transmission difference is ±1 dB or less.

Fig. 2(b) shows the observed FWM results in the graphene-PhCWG sample (red solid), compared with the monolithic silicon-only PhCWG (blue dashed). To avoid the amplified pump and signal transmission submerging the output idler laser spectrum, the pump and signal wavelength are kept at 500 pm detuning. In this example, the pump wavelength is at ~1540 nm. We consider the $G_{idler} = P_{idler}^{output}/P_{signal}^{output}$ by taking the ratio of idler output power and signal output power. This definition can cancel differences caused by any residual fluctuation of the coupling condition. To ensure the FWM is not generated in the auxiliary fibers, the optical spectra before the graphene-PhCWG sample is checked by the OSA and there is negligible idler generated. In addition, for our measurements, we tune the signal laser to TM-polarization which provides more evanescent light interaction with graphene, resulting higher conversion efficiency. The conversion efficiency in graphene-PhCWG is about −23 dB compared to the monolithic silicon-only PhCWG control sample at about −31 dB.

The FWM conversion efficiency, G_{idler}, in the graphene-PhCWG device is described by[11,12]

$$G_{idler} = \frac{P_{idler}}{P_{signal}} = \left(\frac{\gamma^*_{graphene-silicon}\overline{P_p}}{g}\sin h(gL)\right)^2 e^{-\alpha^* L}, \quad (1)$$

where α^* is group index dependent propagation loss of the idler, L is the waveguide length, $\overline{P_p}$ is the effective average pump power (modified by loss α^* along the waveguide length L), and $\gamma^*_{graphene-silicon}$ is the group index dependent nonlinear parameter of the graphene-silicon hybrid, $\gamma^*_{graphene-silicon} = \gamma(n_g/n_0)^2$, $\gamma = 2\pi n_2/A_{eff}\lambda$.[12] Here, A_{eff} is a wavelength-dependent term, with larger cross-section at the slow-light region.[19,24] n_2 is the overall graphene-silicon Kerr coefficient weighted by the E-fields,[4,25] and is computed to be $\sim 7.7 \times 10^{-17}$ m^2/W. Here, g is the parametric gain, described as[11,12]

$$g = \sqrt{\left(\gamma^*_{graphene-silicon}\overline{P_p}\right)^2 - \left(\frac{\Delta K_L + \Delta K_{NL}}{2}\right)^2}, \quad (2)$$

where $\Delta K_L \approx (\Delta\omega)^2\beta_2(\lambda_{pump}) + (\Delta\omega)^4\beta_4(\lambda_{pump})/12$ and $\Delta K_{NL} = 2\gamma^*_{graphene-silicon}\overline{P}_p$ is the linear and nonlinear phase mismatching, respectively. $\Delta\omega = |\omega_{pump} - \omega_{signal}|$, the second and fourth order dispersion parameters ($\beta_2(\lambda)$ and $\beta_4(\lambda)$) can be numerically calculated from the experimental dispersion curve of the device.[11] With the large $\gamma^*_{graphene-silicon}$ (and n_2) and high group index, when we pump at 1540.0 nm and probe at 1540.5 nm, with a simulated FWM conversion efficiency G_{idler} of ~−40 dB matches the experimental result in Fig. 3(a).

The complete experimental and modeled FWM conversion efficiency maps are shown in Figs. 3(a) and 3(b).

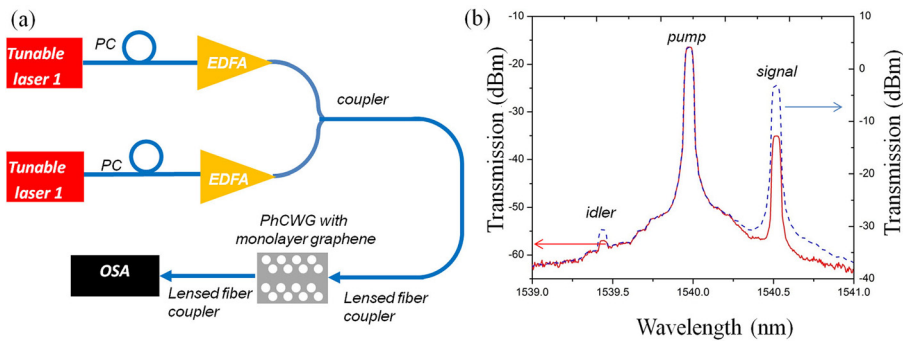

FIG. 2. The schematic of the experimental setup and the output spectra of the FWM before and after graphene is transferred onto PhCWG. (a) The experimental setup schematic diagram for degenerate FWM in graphene-PhCWG; (b) FWM spectra in graphene-PhCWG (red solid) and the control silicon-only PhCWG (blue dashed). The pump wavelength is at ~1540 nm, and the signal detuning is about 500 pm. The FWM conversion efficiency in PhCWG and graphene-PhCWG are about −31 dB and −23 dB, respectively.

Different pump wavelengths, with their group indices dependence, and signal detunings are illustrated. In the measurements, the pump wavelength is tuned from 1534.5 nm to 1540 nm with 500 pm step-sizes and the signal is detuned from the pump between −4 nm and +4 nm with 200 pm step-sizes. The signal-pump detuning is defined as ($\lambda_{signal} - \lambda_{pump}$). The pump and signal powers are kept constant in our measurements at ∼9 dBm. The input power is slightly decreased to avoid the device damage caused by intensity fluctuations when detuning the wavelength. The simulations are modeled in the same optical spectra as the measurements. Both experiments and simulations show that, for each pump wavelength examined (between 1534.5 nm and 1540.0 nm), the conversion efficiency increases as the signal wavelength is red detuned. As noted in Eq. (1) and previous studies,[11,12] the highest conversion efficiency region should be when the signal is detuned for optimal phase matching region and when the group velocity is slowed for increased light-matter interaction. Our measurements and modeling results show an asymmetry in the FWM conversion efficiency because the Graphene-PhCWG chip has an increased propagation loss for the signal or idler light at the mode cutoff (towards the longer wavelengths). For a more clear comparison of the FWM conversion efficiency difference between Graphene-PhCWG and monolithic silicon PhCWG, the pump wavelength is fixed at 1540 nm and the signal is detuned from −3 nm to +3 nm, as shown in Fig. 3(c). When the signal detunes from −1 nm to +1 nm, the FWM conversion efficiency is 3 dB to 6 dB enhanced by graphene. For long detuning wavelength, the conversion efficiency is increased and for short detuning wavelength the conversion efficiency is decreased equal to that in silicon because of the increased loss towards longer wavelengths. Moving into the longer wavelength slow-light region for the pump, the FWM conversion efficiency is somewhat constant due to the tradeoff between the slow-light enhancement and the higher graphene loss in this region. The conversion efficiency of FWM in graphene-PhCWG and PhCWG when the signal detuning is fixed at −0.2 nm and the pump wavelength is tuned from 1536 nm to 1540 nm, as illustrated in Fig. 3(d). Each data point show that the FWM conversion efficiency is about 4 dB enhanced by graphene compared to monolithic silicon-only PhCWG. We note that, with our continuous-wave pump-signal lasers and at our ∼17 dBm coupled-in chip powers, the nonlinear absorption and nonlinear losses are not significant since, when we increased the pump power, the conversion efficiency increased linearly instead of decreasing, as shown in Fig. 4(a). Simulated results of conversion efficiency vs. waveguide length are shown in the inset of Fig. 4(a). The black line shows the FWM conversion efficiency in silicon, which becomes constant when the waveguide length is over 600 μm. The relationships between conversion efficiency of FWM in graphene-PhCWG and waveguide length are indicated by the red curve (graphene absorption 0.05 dB/μm) and blue curve (graphene absorption 0.06 dB/μm). The conversion efficiency increases fast with waveguide length because of the high n_2. And then it drops very fast because the FWM is limited by the high absorption from graphene when the waveguide length increases. This result indicates the graphene-silicon hybrid structure can achieve higher conversion efficiency in a shorter device with the proper band gap engineering to decrease the absorption in graphene. Our further work will focus on this.

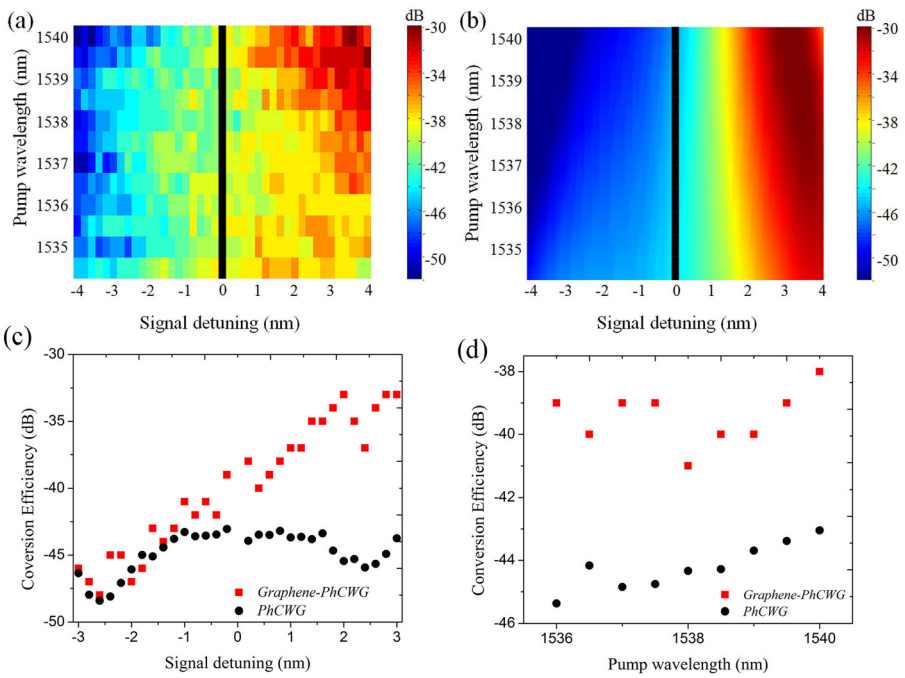

FIG. 3. The experimental and modeling results of the FWM conversion efficiency map and the FWM conversion efficiency difference in graphene-PhCWG and PhCWG. (a) Experimental 2D conversion efficiency map of graphene-PhCWG as a function of pump and signal wavelength, with pump laser from 1534.5 nm to 1540 nm with 500 pm step-sizes. The signal detuning is from −4 nm to +4 nm with 200 pm step-sizes; (b) Corresponding modeling results of the FWM conversion efficiency, with similar pump and signal ranges as the measurements; (c) Different conversion efficiency of FWM in graphene-PhCWG and PhCWG when the pump wavelength is fixed at 1540 nm and the signal is detuned from −3 nm to +3 nm; (d) The conversion efficiency of FWM in graphene-PhCWG and PhCWG when the signal detuning is fixed at −0.2 nm and the pump wavelength is tuned from 1536 nm to 1540 nm.

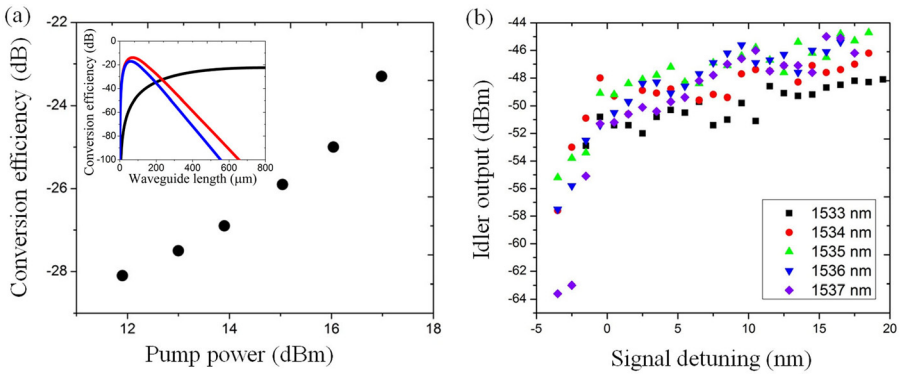

FIG. 4. FWM conversion efficiency varies with the pump power and the waveguide length as well as the idler power varies with signal detuning. (a) Conversion efficiency as a function of pump power (coupled in-chip power) at pump wavelength of 1540 nm; (b) Output idler power as a function of signal detuning at different pump wavelengths. The maximum detuning bandwidth is about 17 nm when the pump wavelength is at 1534 nm. Inset in (a) shows the simulation result of conversion efficiency vs. waveguide length. The black line shows the FWM conversion efficiency in silicon. The relationship between conversion efficiency of FWM in graphene-PhCWG and waveguide length are indicated by the red curve (graphene absorption 0.05 dB/μm) and blue curve (graphene absorption 0.06 dB/μm).

Next, we investigate the 3-dB detuning bandwidth for different signal detunings and for different central pump wavelengths, as shown in Fig. 4(b). We define the whole detuning range over which the idler output power is within 3-dB ($\pm$1.5 dB) of the idler output power measured when the detuning range is +500 pm. (We did not use a 3-dB from the peak FWM conversion efficiency because the FWM conversion efficiency continuously increases for longer wavelengths due to the increased signal and pump scattering loss at the longer (slow-light) wavelengths.) When the signal is detuned to a shorter wavelength than the pump (negative detuning Δ and for smaller absolute values of Δ), there is a sharp decrease in the output idler intensity due to the higher loss in the signal intensity. This higher loss arises from both increased scattering loss in the slow-light region due to minute disorder in the PhC lattice and increased graphene linear absorption. When the signal is detuned to a longer wavelength than the pump (positive detuning Δ and for larger absolute values of Δ), the output idler intensity is somewhat constant due to relatively uniform transmission of the idler in the normal group velocity region—this gives rise to the large FWM bandwidth of 17 nm (at 1534 nm pump). This bandwidth is several times larger than in monolithic silicon PhCWGs. Within this $\approx$17 nm bandwidth, there are local spectral fluctuations due to nonlinear phase-matching.

In this work, we demonstrate the enhanced FWM generation in silicon photonic crystal waveguides with monolayer graphene, in which a $-$23 dB conversion efficiency and a 17 nm 3-dB detuning bandwidth are observed. We experimentally and numerically analyze the effects of graphene enhanced nonlinear coefficients, linear losses, the graphene-PhCWG group indices, and waveguide length on the conversion efficiency. The FWM conversion efficiency can be further improved through engineering and reducing the linear absorption of graphene, for all-optical signal processing in next-generation communication modules.

The authors acknowledge discussions with Junbo Yang, and support from the ONR program on nonlinear dynamics (N000141410041), the National Science Foundation IGERT (DGE-1069240), and the Chinese Scholarship Council.

[1]P. Avouris, Nano Lett. **10**, 4285 (2010).
[2]F. Bonaccorso, Z. Sun, T. Hasan, and A. Ferrari, Nat. Photonics **4**, 611 (2010).
[3]S. J. Koester and M. Li, Appl. Phys. Lett. **100**, 171107 (2012).
[4]T. Gu, N. Petrone, J. McMillan, A. van der Zande, M. Yu, G. Q. Lo, D. L. Kwong, J. Hone, and C. W. Wong, Nat. Photonics **6**, 554 (2012).
[5]Q. Bao, H. Zhang, Y. Wang, Z. Ni, Y. Yan, Z. X. Shen, K. P. Loh, and D. Y. Tang, Adv. Funct. Mater. **19**, 3077 (2009).
[6]F. Xia, T. Mueller, Y.-M. Lin, A. Valdes-Garcia, and P. Avouris, Nat. Nanotechnol. **4**, 839 (2009).
[7]H. Fukuda, K. Yamada, T. Shoji, M. Takahashi, T. Tsuchizawa, T. Watanabe, J.-I. Takahashi, and S.-I. Itabashi, Opt. Express **13**, 4629 (2005).
[8]R. Salem, M. A. Foster, A. C. Turner, D. F. Geraghty, M. Lipson, and A. L. Gaeta, Nat. Photonics **2**, 35 (2007).
[9]R. Espinola, J. Dadap, R. Osgood, Jr., S. McNab, and Y. Vlasov, Opt. Express **13**, 4341 (2005).
[10]M. A. Foster, A. C. Turner, J. E. Sharping, B. S. Schmidt, M. Lipson, and A. L. Gaeta, Nature **441**, 960 (2006).
[11]M. Ebnali-Heidari, C. Monat, C. Grillet, and M. Moravvej-Farshi, Opt. Express **17**, 18340 (2009).
[12]J. F. McMillan, M. Yu, D. L. Kwong, and C. W. Wong, Opt. Express **18**, 15484 (2010).
[13]C. Monat, M. Ebnali-Heidari, C. Grillet, B. Corcoran, B. Eggleton, T. White, L. O'Faolain, J. Li, and T. Krauss, Opt. Express **18**, 22915 (2010).
[14]J. Li, L. O'Faolain, I. H. Rey, and T. F. Krauss, Opt. Express **19**, 4458 (2011).
[15]M. Dinu, F. Quochi, and H. Garcia, Appl. Phys. Lett. **82**, 2954 (2003).
[16]B. Xu, A. Martinez, K. Fuse, and S. Yamashita, paper presented at the CLEO: Science and Innovations (paper CMAA6), May 1–6, 2011.
[17]E. Hendry, P. Hale, J. Moger, A. Savchenko, and S. Mikhailov, Phys. Rev. Lett. **105**, 097401 (2010).
[18]Y. Wu, B. Yao, Y. Cheng, Y. Rao, Y. Gong, X. Zhou, B. Wu, and K. S. Chiang, IEEE Photonic Tech L **26**, 249 (2014), see http://ieeexplore.ieee.org/xpl/articleDetails.jsp?arnumber=6671974.
[19]C. J. Chen, C. A. Husko, I. Meric, K. L. Shepard, C. W. Wong, W. M. Green, Y. A. Vlasov, and S. Assefa, Appl. Phys. Lett. **96**(8), 081107 (2010).
[20]N. Petrone, C. R. Dean, I. Meric, A. M. Van Der Zande, P. Y. Huang, L. Wang, D. Muller, K. L. Shepard, and J. Hone, Nano Lett. **12**, 2751 (2012).
[21]X. Li, W. Cai, J. An, S. Kim, J. Nah, D. Yang, R. Piner, A. Velamakanni, I. Jung, and E. Tutuc, Science **324**, 1312 (2009).
[22]W. Zhao, P. H. Tan, J. Liu, and A. C. Ferrari, J. Am. Chem. Soc. **133**, 5941 (2011).
[23]A. C. Ferrari, J. C. Meyer, V. Scardaci, C. Casiraghi, M. Lazzeri, F. Mauri, S. Piscanec, D. Jiang, K. S. Novoselov, S. Roth, and A. K. Geim, Phys. Rev. Lett. **97**, 187401 (2006).
[24]L. O'Faolain, S. A. Schulz, D. M. Beggs, T. P. White, M. Spasenović, L. Kuipers, F. Morichetti, A. Melloni, S. Mazoyer, and J.-P. Hugonin, Opt. Express **18**, 27627 (2010).
[25]S. Afshar V and T. M. Monro, Opt. Express **17**, 2298 (2009).